ELSEVIER

Biophysical Chemistry 125 (2007) 127–137

Biophysical Chemistry

http://www.elsevier.com/locate/biophyschem

Exploration of the conformational space of myosin recovery stroke via molecular dynamics

Hyung-June Woo *

Department of Chemistry, University of Nevada, Reno, NV 89557, United States

Received 15 June 2006; received in revised form 1 July 2006; accepted 1 July 2006
Available online 11 July 2006

Abstract

Muscle contractions are driven by cyclic conformational changes of myosin, whose molecular mechanisms of operation are being elucidated by recent advances in crystallographic studies and single molecule experiments. To complement such structural studies and consider the energetics of the conformational changes of myosin head, umbrella sampling molecular dynamics (MD) simulations were performed with the all-atom model of the scallop myosin sub-fragment 1 (S1) with a bound ATP in solution in explicit water using the crystallographic near-rigor and transition state conformations as two references. The constraints on RMSD reaction coordinates used for the umbrella sampling were found to steer the conformational changes efficiently, and relatively close correlations have been observed between the set of characteristic structural changes including the lever arm rotation and the closing of the nucleotide binding pocket. The lever arm angle and key residue interaction distances in the nucleotide binding pocket and the relay helix show gradual changes along the recovery stroke reaction coordinate, consistent with previous crystallographic and computational minimum energy studies. Thermal fluctuations, however, appear to make the switch-2 coordination of ATP more flexible than suggested by crystal structures. The local solvation environment of the fluorescence probe, Trp 507 (scallop numbering), also appears highly mobile in the presence of thermal fluctuations.

Keywords: Motor protein; Myosin; Muscle contraction; Power stroke; Molecular dynamics; Free energy

1. Introduction

Free energy transductions between chemical and mechanical forms underlie a wide variety of key processes in biological cells, including the transport of biochemical cargoes, ATP synthesis, RNA synthesis during transcription, and muscle contractions. One of the most well-characterized family of motor proteins are myosins, the actin-based motors driving the sliding movements of thick and thin filaments during muscle contractions [1].

A widely accepted working model of actomyosin operations, first proposed based on biochemical studies [2] and later refined to incorporate crystallographic structural information [3–5], is the swinging lever arm mechanism, where a myosin head (or S1, the catalytically active minimal unit) attached to the thick filament by the lever arm can adopt at least two distinct stable conformations, distinguished by both the orientation of the lever arm and the local conformation of the nucleotide binding pocket. The stable state of a myosin head bound to an actin filament without nucleotide is the *rigor* conformation, characterized by the "down" orientation of the lever arm and the nucleotide binding pocket "open" [6]. High-resolution crystal structures of the rigor actomyosin complexes are currently unavailable, for which cryo-EM studies [7–9] have thus been playing major roles in structural investigations. In particular, the rigor conformation is thought to differ considerably from the *near-rigor* state [10], the stable conformation of a nucleotide-free myosin head detached from the actin filament [Fig. 1(a) and (c)]; the upper 50 K domain is rotated in a near-rigid-body fashion relative to the lower 50 K domain, closing the major cleft between the two domains to facilitate actin–myosin binding while opening the nucleotide binding pocket [9]. A binding of ATP into the actin-bound rigor S1 leads to the dissociation of the myosin head into the solution, after which the lever arm is thought to be re-primed into the "up" orientation [Fig. 1(a)→(b)], accompanied by the closing of the nucleotide binding pocket [Fig. 1(c)→(d)]. The end-state of this conformational

* Tel.: +1 775 784 1406; fax: +1 775 784 6804.
E-mail address: woo@unr.edu.

0301-4622/$ - see front matter © 2006 Elsevier B.V. All rights reserved.
doi:10.1016/j.bpc.2006.07.001

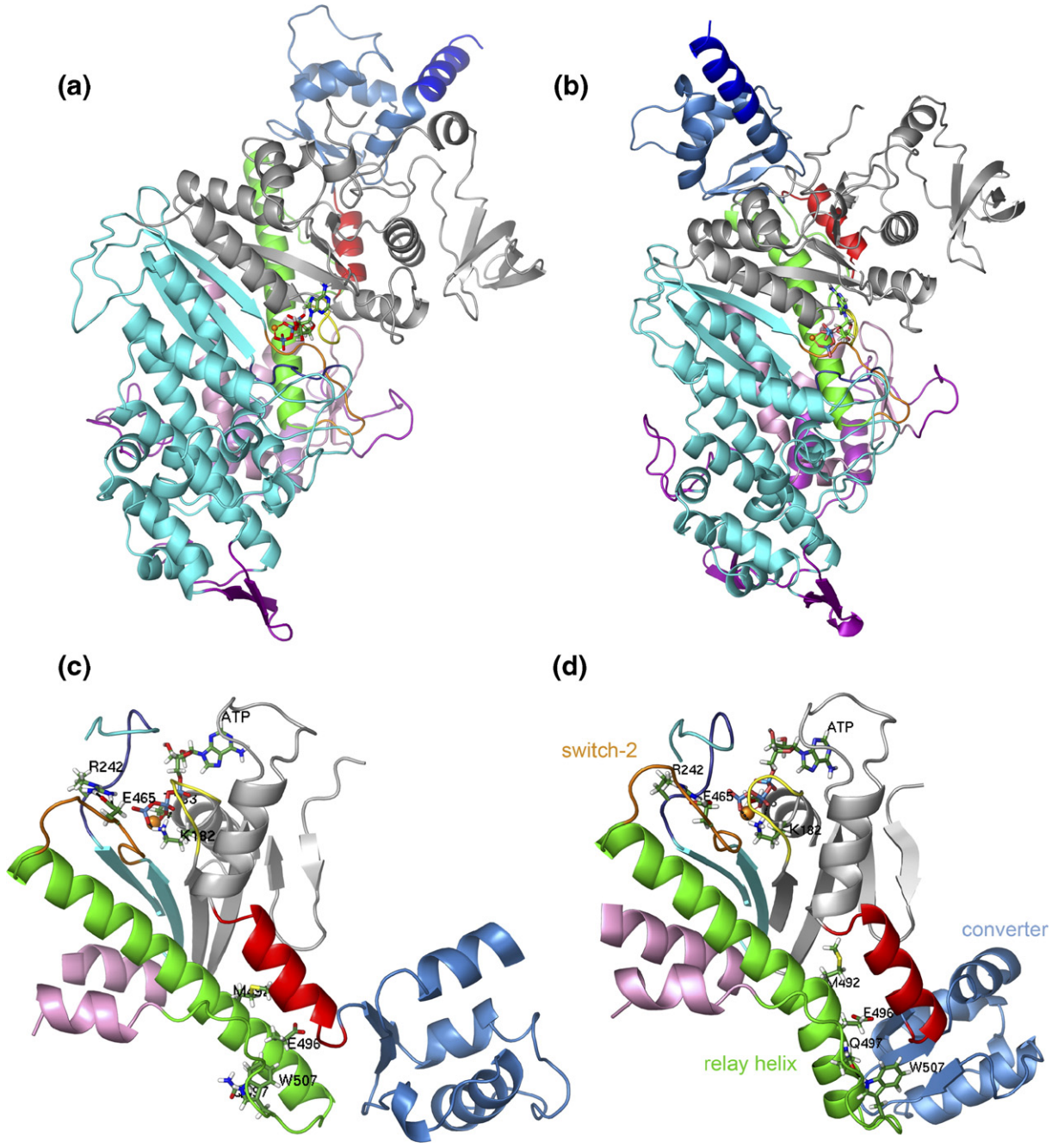

Fig. 1. Two end-point conformations of the re-priming step from simulations. (a)–(b) Arrangement of sub-domains in the (a) R and (b) P-states. The actin filament axis is directed horizontally. (c)–(d) Close up views of the binding pocket and the converter/lever arm in the (c) R and (d) P-states. Colors used are as follows: upper 50 K (cyan), lower 50 K (pink), actin-binding regions (purple) [25], converter (sky blue), lever arm (blue), relay region (green), N-terminal domain (silver), SH1 helix (red), switch-1 (dark blue), switch-2 (orange), and P-Loop (yellow). ATP and some of the key residues are shown in sticks, and the magnesium ion as an orange sphere. Lys 182 and Thr 183 remained close to the γ-Pi throughout the trajectories. (For interpretation of the references to colour in this figure legend, the reader is referred to the web version of this article.)

change, referred to as the re-priming or recovery stroke, corresponds to the *transition-state* (or *pre-stroke*) conformation [11], modeled by the crystallographic structures of S1 with ATP-analogs such as ADP·VO_4 [12,13] [Fig. 1(b) and (d)]. The nucleotide binding pocket consists of several well-conserved structural motifs playing essential roles in ATP-hydrolytic activities of myosin and other related ATPases such as G-proteins, including the switch-1 and switch-2 domains [3,12]. The closed conformation of the binding pocket is characterized by the approach of the switch-2 toward the γ-phosphate (Pi) of ATP. The concurrent conformational changes put into place key catalytic residues of the hydrolysis reaction, thereby "turning on" the ATP hydrolysis activity of S1.

The release of Pi after hydrolysis is believed to be the key event triggering the work production step, the *power stroke*, which is facilitated by the weak re-association of the transition-

state myosin–ADP·Pi complex with the actin filament. It is natural to suppose that the power stroke would be closely related to the recovery stroke, only reverse in direction, in which the lever arm is restored into the "down" orientation of the rigor state and the nucleotide binding pocket is re-opened [Fig. 1(b)→(a) and (d)→(c)]. Details of molecular level structural changes involved in the power stroke, however, await more direct structural information of actin-bound myosins.

With the prominent global structural changes including the large lever arm re-orientation and the well-characterized two end-states of crystallographic structures, the recovery stroke provides an ideal part within the overall muscle contraction cycle that could potentially be amenable to dynamical and energetic characterizations beyond the structural level. Steffen and Sleep [14] recently used single-molecule optical force measurement techniques to show that the recovery stroke primarily occurs while dissociated from actin as in the original Lymn–Taylor mechanism [2], as opposed to the alternative Eisenberg–Greene proposal [15] where the lever arm is argued to be re-primed after ATP binding with the post-stroke myosin head still bound to actin.

Most recently, Fischer et al. [16] have performed a computational study of the myosin recovery stroke using the conjugate peak refinement method to obtain a minimum energy path connecting the near-rigor and pre-stroke states in the conformational space, delineating in remarkable detail a sequence of structural states constituting the recovery stroke. As has been suggested based on comparisons of the two end-point crystallographic structures, the recovery stroke is dominated by the rigid-body-type rotation of the converter domain/lever arm complex, which is closely coupled to the translational pulling and the kink formation of the relay helix, caused in turn by the closing of the nucleotide binding pocket and the approach of the switch-2 toward the γ-Pi [Fig. 1(c) and (d)].

Molecular modeling techniques including the MD simulations can potentially offer avenues of detailed studies that can complement structural information. Zheng and Brooks [17,18] have applied the normal mode analysis to the elastic network model of motor proteins [19,20], and Minehardt et al. [21] have used the mixed classical/quantum mechanical methods to study the interaction of ATP with myosin binding site catalytic residues. Lawson et al. [22] have performed MD simulations to consider the structural features of the local conformational spaces of binding site and Pi-release pore of myosin. Li and Cui have used the quantum mechanical/molecular mechanical method [23] to study the coupling of conformational degrees of freedom in the myosin nucleotide binding pocket with the ATP hydrolysis reaction, and the normal mode analysis [24] to consider the structural flexibilities of a myosin head coupled to its enzymatic activity. There has also been a recent MD study of the protein–protein interactions of the chicken skeletal myosin head with actin monomers [25] at the residue-level, based on the cryo-EM model of Holmes et al. [9,26].

Building on such previous works of structural and simulation studies of myosin conformational states, the results of a set of umbrella sampling MD simulations are reported in this paper that connects the near-rigor and transition-state conformations of ATP-bound S1 in solution, aimed at illuminating the energetics of the structural transitions constituting the recovery stroke. The umbrella sampling MD for calculations of the free energy profiles (or potential of mean force) [27,28], when combined with more coarse-grained stochastic dynamical descriptions [29,30], offers a powerful method to bridge the time scale gap between the range accessible by unconstrained simulations (nanoseconds) and the typical time scales of large conformational changes such as those involved in motor protein operations (up to or beyond milliseconds), as has successfully been applied recently to a variety of biomolecular systems [31–36]. In umbrella sampling simulations, with an appropriate choice of reaction coordinates, one imposes constraining potentials to bias the free energy, allowing efficient samplings of conformational spaces normally inaccessible [37]. The weighted histogram analysis method [38–40] then can be used to unbias the collected histograms and combine multiple simulation data to yield the free energy. As a first step toward such calculations of myosin recovery stroke, the work reported here is focused on evaluating the efficiency of one possible choice of reaction coordinates, and considering the energetics of the previously identified structural transitions associated with the recovery stroke using the umbrella sampling trajectories.

The choice of appropriate reaction coordinates is often crucial to the success of the free energy MD method, and in this work, the root mean square deviation (RMSD) with respect to two reference structures as the set of reaction coordinates was adopted, following Banavali and Roux who pioneered the methodology in their recent studies of the A and B-DNA conformational free energy landscapes [33] and the signaling mechanism of Src kinase Hck [34]. The resulting data have also been analyzed to examine the correlation of the reaction coordinates with structural changes characteristic of our system such as the lever arm angle. In particular, the set of umbrella sampling trajectories with harmonic constraints closely spaced in the RMSD reaction coordinate space can be regarded as a set of multiple steered (or targeted) MD [41–43] widely used to study conformational changes of proteins too slow to be simulated with unconstrained simulations. The analysis of the sampled trajectories thus yield a wealth of structural information associated with the recovery stroke that includes the effects of thermal fluctuations.

2. Methods

All simulations and analysis were performed using the c31b1 version of CHARMM [44] with the version 22 all-atom force fields [45]. The scallop myosin S1 initial structures were built using the crystal structure without nucleotide (PDB ID 1KK7 [10]; R-state; RMSD with respect to this structure denoted as y_1), and the ADP·VO_4-bound structure (PDB ID 1QVI [11]; P-state; RMSD with respect to this structure denoted as y_2). The lever arm beyond Ala 787 was truncated to reduce the overall system size of the solvated S1. The γ-Pi position was taken as the vanadium coordinate of the original P-state crystal structure. Missing residues in disordered loops were built by interpolating backbone positions between nearest residues with known coordinates.

Unknown side-chain heavy atom coordinates were then built using Swiss-PdbViewer [46]. Hydrogen atom coordinates were added using HBUILD of CHARMM [44], followed by short energy minimizations to correct unphysical coordinates of the built backbone and side-chain atom positions with the known crystal structure coordinates fixed. Potassium atoms were added to make the overall charge of the systems neutral for each window. The chains were then solvated in pre-equilibrated water box in orthorhombic geometry. The TIP3P model [47] was used for water molecules. A typical box geometry after equilibration was approximately $140\times120\times80$ Å^3, whose volume usually dropped initially in the constant pressure dynamics to reach equilibrium values within tens of picoseconds. The total number of water molecules was approximately 37,500 (the numbers differed slightly for different windows) and the total number of atoms 125,000 on average.

Umbrella sampling simulations were performed for 16 windows with ATP in the binding pocket, each under the set of harmonic constraining potentials,

$$u(y_1,y_2) = k(y_1-\bar{y}_1)^2 + k(y_2-\bar{y}_2)^2, \quad (1)$$

where k is the force constant and the reference offset values $\bar{y}_1, \bar{y}_2$ of the RMSD with respect to the crystal structures were equally spaced along the diagonal line of Fig. 5 as shown in Table 2. All RMSD values were calculated within the set of 5,473 non-hydrogen atoms common to the original R and P-state crystal structures with known coordinates. The RMSD constraints in each window were imposed using the CONS module of CHARMM. The simulations were performed with constant pressure (1 atm) and temperature (300 K) dynamics [48–50] with the time step of 2 fs in periodic boundary conditions using the particle mesh Ewald method [51] for electrostatics, and the van der Waals interaction cutoff of 10 Å. The SHAKE algorithm [52] was used to fix bond lengths involving hydrogen atoms. The protein center-of-mass was harmonically held at the box center with a force constant of 1 kcal/mol Å^2 to prevent the overall drifting of the molecule. For each window, the initial structures for sampling were generated by equilibration runs of typically 0.1 ns length with the force constant of 100 kcal/mol Å^2, started from the P-state reference coordinate. Subsequent samplings were run with the constraints Eq. (1) with force constant 1 kcal/mol Å^2. The speed of the dynamics sampling was approximately 0.63 ps/h on a 3.0 GHz Intel Xeon chip run serially. Parts of the simulations were also run in parallel (16 processors per window) on Alpha EV6.8CB processors, for which the speed of dynamics was approximately 3.86 ps/h.

Table 1
Sub-domains of myosin S1 (scallop myosin numbering; lever arm truncated beyond Ala 787) and RMSD between the two reference (near-rigor and pre-stroke) crystal structures calculated within each sub-domain

	Residue number	RMSD (Å)
Total	1–787	8.60
N-terminal	1–199, 663–694	1.27
Upper 50 K	200–460, 602–642	1.39
Lower 50 K	516–601, 643–662	1.24
Converter	708–774	1.41
Lever arm	775–787	0.86
Relay region	471–515	4.22
Switch-1	237–243	1.58
Switch-2	461–470	1.34
P-loop	176–180	0.30
SH1 helix	695–707	2.40

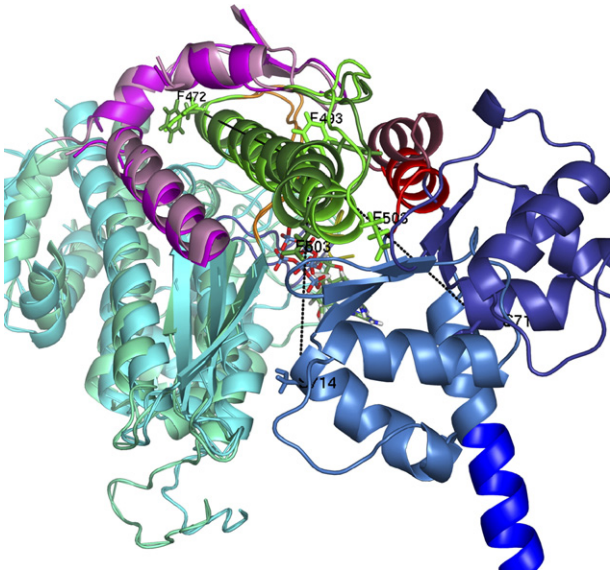

Fig. 2. A different view of the conformational change, where the two states are shown aligned using S1 atoms excluding the converter/lever arm. The darker shades of colors for each sub-domain represent the P-state conformation. The figure also shows the lever arm angle, defined as the dihedral formed by centers-of-mass of Ser 714, Phe 493, Phe 472, and the S1 excluding the converter/lever arm. The angle of relay helix kink was defined as that formed by the centers-of-mass of Phe 472, Phe 493, and Glu 503. (For interpretation of the references to colour in this figure legend, the reader is referred to the web version of this article.)

For the steered MD results, the trajectory was started from a late stage output coordinate of the window 1 (Table 2), which corresponds to the conformational region closest to the R-state. A transient dynamics was then run with the harmonic constraining potentials corresponding to the window 16, first with a weaker force constant of 1 kcal/mol Å^2 for 0.8 ns and then with 10 kcal/mol Å^2 for 0.45 ns.

The two-dimensional weighted histogram analysis was done using a code written by the author implementing the algorithm in Refs. [39,40] with the grid size of 0.2 Å in each dimension. The free energy landscape of Fig. 5 was obtained by using the trajectory segments excluding the first 0.1 ns, unbiased using the weighted histogram analysis. In obtaining the statistics of the progression of structural signatures shown in Fig. 6, angle and distance data were collected using y_2-value filters of 1 Å width around the minimum free energy path $y_2(\lambda)$ along the diagonal path in Fig. 5, and processing the trajectory segments.

3. Results

3.1. Myosin conformational changes and sub-domain rearrangements

One of the common features of native protein conformational changes related to functional regulations is the dominance of

rigid-body-type relative rearrangements of sub-domains, such as the hinge and shear motions [53], which provide economical repertoire of low energy inter-conversion routes between different functional states. The structural features of myosin head inferred from crystallographic structures point to the major roles played by such rigid-body rearrangements of sub-domains [3]. The scallop myosin was chosen as the model system for this study, for which up to three (near-rigor; R, pre-stroke; P, and the internally uncoupled) distinct conformational states have been identified via crystallography [11,54,55]. The sub-domains of the scallop myosin S1 are illustrated in Fig. 1 and listed in Table 1. The RMSD shown in Table 1 are the values between the two reference crystal structures (R and P-states) calculated within each sub-domain as measures of the structural rigidity during the conformational change. The overall S1 conformational change is massive (8.60 Å), whereas most of the corresponding RMSD in sub-domains are much smaller, indicating that the sub-domains scarcely change their folds while rigidly moving relative to one another. A bulk of the over-all conformational change is in fact accounted for by the rigid rotation of the converter domain/lever arm complex with respect to the rest of S1 body (Fig. 2) [3,10,11,16], evidenced by the RMSD of 2.77 Å between the two references for the S1 body excluding the converter/lever arm and relay region. The largest intra-domain conformational change is seen to occur within the relay region, reflecting the characteristic kink formation [3,16] [Fig. 1(d)] in the relay helix accompanying the recovery stroke.

3.2. RMSD as reaction coordinate and steered MD

The large difference between the overall and partial RMSD values for the reference structures shown in Table 1 suggests that the RMSD itself might serve as an efficient reaction coordinate [33,34] for biasing the sampling of conformational states traversing the recovery stroke. To examine the efficiency of umbrella sampling simulations using the RMSD as the constrained reaction coordinate, two terminal window trajectories of the overall sampling sets (see below) were chosen for testing the convergence

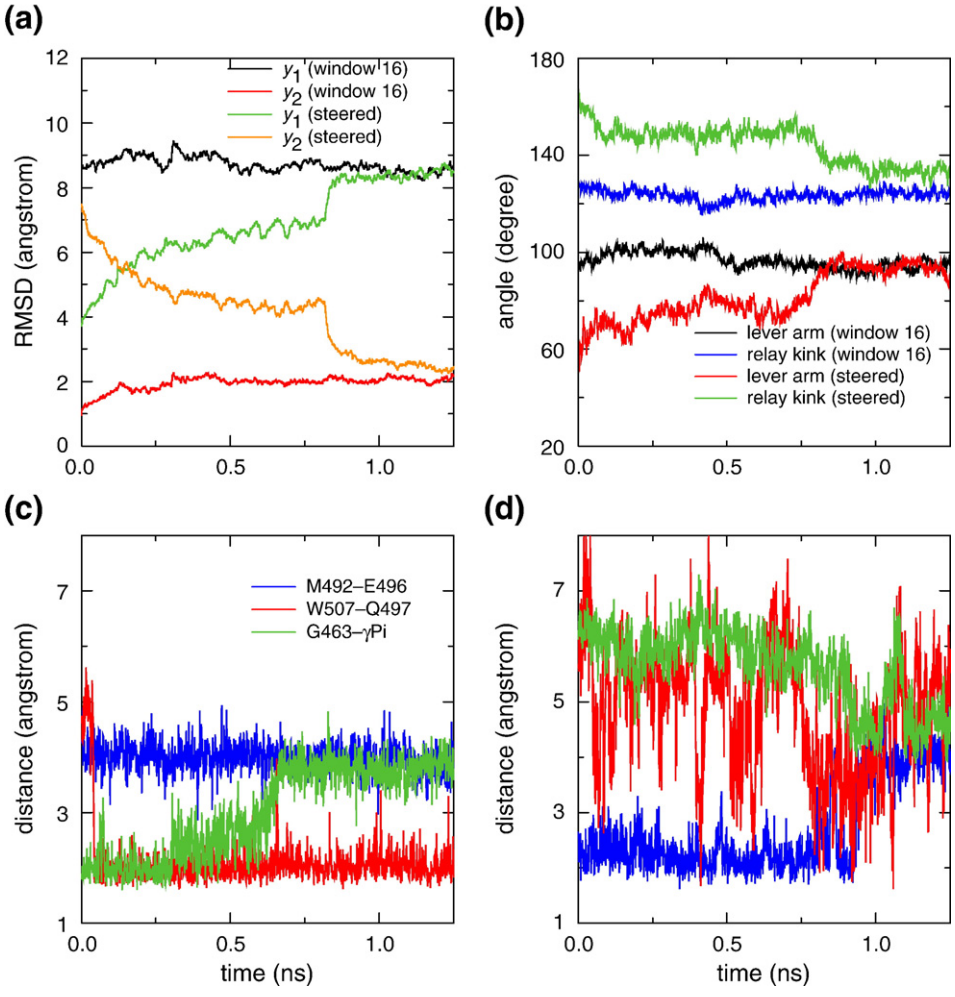

Fig. 3. Cross-window steered MD using RMSD reaction coordinates y_1 and y_2 with varying strengths of constraining potentials, compared with the umbrella sampling data of the window 16 in Table 2. (a) RMSD time-series. (b) The corresponding time-series of the lever arm rotation and relay helix kink angles of the window 16 and the steered MD trajectory. (c) The backbone hydrogen bond distance between Met 492 and Glu 496, which breaks to produce the kink in the P-state, the hydrogen bond distance between the fluorescence probe Trp 507 and Gln 497, and the switch-2 Gly 463–γ-Pi distance for the window 16 trajectory. (d) The same set of structural signature time-series for the steered MD trajectory, shown with the same colors as in (c). (For interpretation of the references to colour in this figure legend, the reader is referred to the web version of this article.)

Table 2
Umbrella sampling schemes and statistics

Window	$\bar{y}_1$ (Å)	$\langle y_1 \rangle$ (Å)	$\bar{y}_2$ (Å)	$\langle y_2 \rangle$ (Å)	Time (ns)
1	0.54	3.20±0.35	8.06	7.57±0.22	3.24
2	1.08	3.29±0.37	7.53	7.34±0.60	3.72
3	1.61	4.33±0.34	6.99	6.54±0.34	3.20
4	2.15	3.73±0.33	6.45	6.78±0.28	2.55
5	2.69	5.20±0.44	5.91	5.05±0.46	3.00
6	3.23	5.70±0.37	5.38	4.69±0.31	1.96
7	3.76	6.02±0.89	4.84	4.39±0.66	2.64
8	4.30	7.50±0.35	4.30	2.85±0.34	2.69
9	4.84	6.90±0.98	3.76	4.60±0.95	2.60
10	5.38	7.41±0.35	3.23	3.03±0.20	2.81
11	5.91	7.76±0.27	2.69	2.45±0.22	2.89
12	6.45	8.00±0.62	2.15	2.62±0.40	2.39
13	6.99	8.07±0.49	1.61	2.64±0.24	2.54
14	7.53	8.68±0.29	1.08	2.24±0.27	2.83
15	8.06	8.74±0.18	0.54	2.13±0.13	2.51
16	8.60	8.62±0.23	0.00	2.07±0.13	2.67
Total					44.2

$\bar{y}_1$ and $\bar{y}_2$ refer to the location of the minimum of constraining potentials. The average and standard deviation values were calculated for each time-series excluding the initial 0.1 ns. The time is the total length of the trajectories for each window.

of the sampling using two different magnitudes of harmonic force constants (Fig. 3). The resulting transient trajectory, along with those taken from the set of umbrella sampling data, can be regarded as exploratory steered (or targeted) MD trajectories [41–43,56–59].

Fig. 3 shows the time-series data of the RMSD y_1 (the value with respect to the R-state) and y_2 (the value with respect to the P-state) relative to the two reference structures along with a number of structural parameters characteristic of the recovery stroke. The two RMSD reaction coordinates show monotonic and smooth evolutions, although it appears that a complete crossover from the window 1 to window 16 with the force constant of 1 kcal/mol Å^2 would take multiple nanoseconds. Trajectories run in the presence of constraints with larger offset RMSD values, $\bar{y}_1$ and $\bar{y}_2$ in Eq. (1), necessarily sample larger volumes of conformational space than those with smaller offset, whereas the free energy as a function of RMSD invariably diverges in the limit of zero RMSD due to the entropic cost of quenching conformational fluctuations. Therefore, the equilibrated time-series of the window 16 in Fig. 3 (a) shows large positive deviations of y_2 and smaller deviations of y_1 from their offset values, a generic trend observed in terminal windows. The convergence of y_2 for the steered trajectory is thus targeted toward a much smaller set of conformational states, resulting in the relatively slower convergence. However, with stronger force constants to accelerate the convergence as in the cross-window steered MD shown in Fig. 3 and in the preparation and sampling of trajectories (Table 2), few signs of hysteresis were observed, supporting the notion that the overall conformational changes of the recovery stroke largely consist of unhindered rigid-body-type rearrangements of sub-domains, which can efficiently be steered with the constraining potentials using RMSD reaction coordinates.

Specific structural changes during the transition from the R-state to P-state in the steered trajectory are also shown in Fig. 3(b) and (d). The lever arm is seen to be gradually re-primed by about 40° diffusively, which becomes almost complete after the first 0.8 ns with the weaker force constant, indicating that the structural rearrangement forced by the weaker constraint mainly consists of the rotation of the lever arm/converter domain. More subtle structural changes [3] [Fig. 1(d)], including the kink formation of the relay helix [Fig. 3(b)], the approach of the switch-2 (Gly 463) toward the γ-Pi, and the hydrogen bond formation of the fluorescence probe Trp 507 with Gln 497 [60–63], are seen to be accelerated by the stronger constraint [Fig. 3(d)]. It is also notable that within the window 16 trajectory in Fig. 3(c), the Gly 463-γ-Pi hydrogen bond, initially formed during the preparation stage with force constant of 100 kcal/mol Å^2, soon weakens into ~4 Å during the production run. The relative weakness of the approach of the switch-2 toward ATP in the sampling of conformational spaces (with the non-hydrolyzable ATP of classical force fields) appears generic.

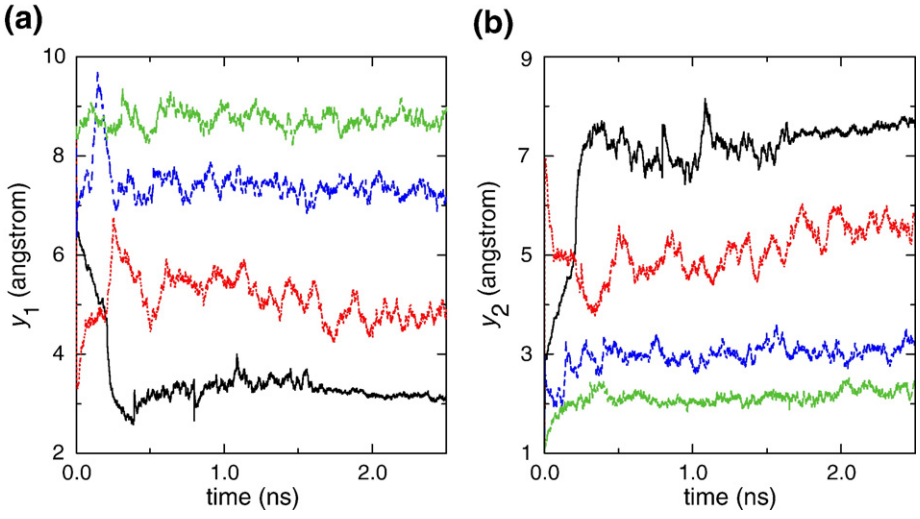

Fig. 4. A few examples of umbrella sampling time-series. (a) and (b) show the RMSD y_1 and y_2 with respect to the near-rigor and transition state reference structures, respectively. The solid (black), dotted (red), dashed (blue), and long-dashed (green) lines are the data from the window 2, 5, 10, and 15, respectively (Table 2). (For interpretation of the references to colour in this figure legend, the reader is referred to the web version of this article.)

3.3. Umbrella sampling of the conformational space

Umbrella samplings of the conformational space were performed with 16 windows, simulated with harmonic constraining potentials centered on the diagonal of the y_1–y_2 plane (Table 2). The simulations yielded a series of conformational ensembles connecting the R and P-states, whose representative snapshots from the two end-point windows are shown in Fig. 1. Fig. 4 shows a few selected time-series data of the two RMSD reaction coordinates from the umbrella sampling. The relative amount of deviations of the average RMSD from the offset values, on top of the entropy-related generic trends discussed in the previous sub-section, can be regarded as the measure of the thermodynamic stability of the conformational states represented by the region in the reaction coordinate space. Inspections of Fig. 4 indicate that y_1 shows much larger positive deviations from the values forced by the constraints than y_2, a feature that was consistently observed in the sampling data. The qualitative feature of the biased stability towards the P-state conformation is consistent with the fact that the reference state is the crystal structure of S1 with bound ATP.

With sufficient amount of sampling, the weighted histogram analysis [39] of the umbrella sampling data can ultimately allow one to quantify the conformational changes thermodynamically. With the aim of assessing the feasibility of extracting the free energy landscape from such umbrella sampling data, we analyzed the collected histogram to obtain the two-dimensional free energy landscape (Fig. 5). The general topography of the landscape appear to be characterized by a monotonic decrease of free energy along the diagonal pathway sampled. The neighborhood of the P-state, in particular, is comparatively flat, exhibiting a wide plateau rather than a sharp minimum.

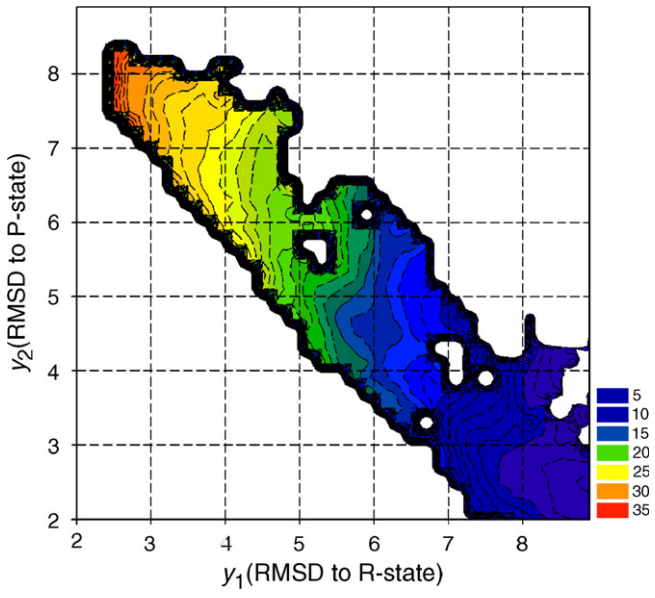

Fig. 5. The two-dimensional conformational free energy landscape obtained by the weighted-histogram analysis of the umbrella sampling data. The contour levels are in units of kcal/mol. (For interpretation of the references to colour in this figure legend, the reader is referred to the web version of this article.)

3.4. Progression of structural changes

To examine the progression of structural changes believed to accompany the myosin recovery stroke [16] within the dynamical simulation data that includes effects of thermal fluctuations, statistics were collected for suitably defined structural signatures along the diagonal pathway shown in Fig. 5. As can be inferred from Table 1, the overall conformational change is dominated by the rigid-body rotation of the converter/lever arm complex. The rotation angle exhibits monotonic and gradual changes up to ~80° with relatively small fluctuations [Fig. 6(a)], which indicates that the RMSD coordinates are closely coupled to the rigid-body rotation angle of the lever arm/converter domain complex. The angle is defined to be zero for the R-state crystal structure, and as shown in Fig. 6, there is no sampling of the angular range 0°~20° despite the constraints, which suggests that the particular lever arm angle adopted by the S1 in the R-state crystal structure might be unstable in the presenceof ATP.

The development of the relay helix kink, caused by the steric constraints due to the "pulling" of the helix by switch-2 during the closing of nucleotide binding pocket [Fig. 1(c)→(d)], is also gradual along the reaction coordinate, producing a ~30° kink angle at the end. However, the local dislocation of the helix manifested as the breakage of backbone hydrogen bond between Met 492 and Glu 496, is abrupt, near $\lambda = 0.3$ where $0 \le \lambda \le 1$ parametrizes the progression on the one-dimensional projection of the reaction coordinates, in close agreement with the results of the minimum energy study of Fischer et al. [16].

With the nucleotide binding pocket closed and switch-2 coordinating the ATP, the amide group of Gly 463 in the switch-2 and γ-Pi forms a hydrogen bond in the P-state crystal structures. The Gly 463-γ-Pi distance rapidly drops from 6 Å to 4±1 Å near $\lambda \simeq 0.3$. However, it then shows oscillations in its average values as λ increases, reaching ~5±1 Å near $\lambda = 1$. The flexible nature of the Gly 463-γ-Pi hydrogen bond, also indicated in the spontaneous dissolution of the bond in the window 16 time-series shown in Fig. 3(c), suggests that thermal fluctuations might play important roles in the conformational stability of the ATP binding residues. However, it is also worth noting that implications to the real ATP-bound S1 conformations might be limited since classical force fields forbid hydrolysis in the current simulations, which could significantly alter the relative stability of the local conformational states near the end-point P-state. It is nevertheless possible to envision detailed comparisons with experiments probing the distribution of conformational states using ATP analogs such as ATP·VO_4.

The salt-bridge between Arg 242 of switch-1 and Glu 465 of switch-2, known to play essential roles in catalytic activities of myosin [60,64], practically remained immobile throughout the trajectories with little appreciable fluctuations [Fig. 6(b)]. In the near-rigor crystal structures, the switch-2 is located away from the binding pocket with the salt-bridge broken [3,10]. The current results indicate that once ATP is bound, the salt-bridge is essentially immutable energetically. Its formation thus might constitute a fast step initiating the closing of the binding pocket, which is also consistent with the observation reported in Fischer et al. [16] that energy minimizations with a bound ATP starting

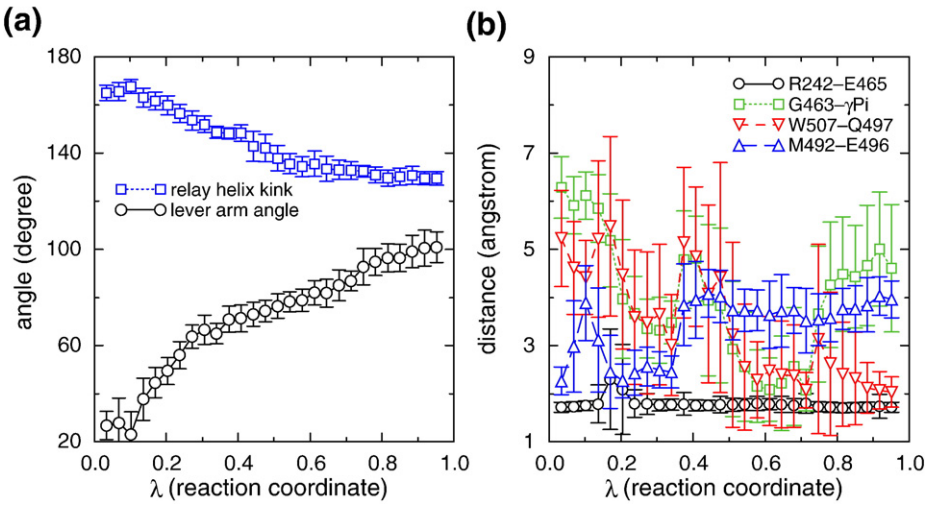

Fig. 6. Statistics of the progression of structural signatures of the recovery stroke. (a) Lever arm and relay helix kink angles. The lever arm rotation angle was measured relative to the crystal R-state value taken as zero, and the angle of relay helix kink is 180° when the helix is straight (Fig. 2). (b) Key residue interaction distances in the binding pocket along the diagonal pathway. Hydrogen bond lengths are the minimum hydrogen-heavy atom distances among structurally equivalent pairs where applicable. Error bars represent $\pm\sigma$.

from the R-state crystal structure of *Dictyostelium* S1 lead to a spontaneous formation of the salt bridge. The salt-bridge is thus strongly favored energetically even close to the R-state conformation when ATP is present.

The fluorescence of Trp 507 (Fig. 2) has been used often as a probe of the S1 conformational change including the recovery stroke, where a rapid initial quench of the fluorescence intensity upon ATP binding is usually followed by a slow enhancement [3,65]. In the crystal structures of pre-stroke S1, Trp 507 forms a tight hydrogen bond with Gln 497. The hydrogen bond distance decreases to about 3 ~ 4 Å around $\lambda \simeq 0.3$ [Fig. 6(b)], but appears highly flexible up to $\lambda \simeq 0.9$, after which the length reaches 2 Å with a sharp quench of fluctuations.

4. Discussion

The results reported here provide complementary evidences and verifications of the structural changes associated with the recovery stroke identified in crystallographic [3] and minimum energy studies [16]. The all-atom simulation data obtained support the expectations based on crystallographic studies [10,11] that the rigid-body rearrangements dominate global conformational changes of myosin head. It also provides indirect supports for more coarse-grained mechanical models of motor proteins which are based on considerations of such rigid-body sub-domain motions [66,67]. The constrained dynamics of RMSD reaction coordinates allows one to accelerate the sampling of structural changes connecting the two distant endpoint conformations. The statistics of the structural progressions obtained here also add the effects of thermal fluctuations inaccessible in crystallographic and minimum energy studies, and in particular show that larger scale conformational changes, such as the lever arm rotation, tend to exhibit gradual and monotonic changes, while local structural changes at the residue-level can often range from highly disordered (Gly 463–γ-Pi hydrogen bond) to essentially frozen (Arg 242-Glu 465 salt-bridge).

Although the actual conformational pathways the protein traverses during the recovery stroke might differ from the diagonal path sampled in Fig. 5, the sampled path nevertheless constitutes one of the strong candidates for such actual pathways, which is also supported by the close agreement of the structural transitions identified along the path (Fig. 6) with the minimum energy study by Fischer et al. [16]. The precise energetics of the pathway, however, is more difficult to ascertain, since free energy MD samplings typically converge slowly. In particular, the absolute value of the free energy difference indicated in the landscape shown in Fig. 5 is larger than expected, and an analysis of the convergence properties of the free energy values indicated that their magnitudes are gradually decreasing over the course of sampling performed. Substantially longer simulations would be necessary to establish quantitatively the nature of the overall free energy landscape of the recovery stroke.

Comparisons with both existing and future experimental studies can play key roles in such considerations of the energetics of conformational changes. Results of biochemical mutagenesis approaches can be used for such purposes. The Arg 242-Glu 465 salt-bridge, for example, has previously been shown with mutagenetic studies [60,64] to be essential to the ATPase activity of myosin. The computational results indicating the extraordinary stability of the salt-bridge agree well with such experimental findings. Among other modern single-molecule techniques, the fluorescence resonance energy transfer (FRET) methods can potentially provide data directly reflecting the dynamics as well as nonequilibrium statistics of the conformational changes [68]. The qualitative trends of the free energy landscape shown in Fig. 5, for example, are consistent with the FRET-based studies of myosin recovery and power strokes in solution [69,70], where it has been shown that a rapid relative approach of the FRET donor/acceptor pair labels on the C and N-termini of S1 (signifying the recovery stroke) occurs upon an addition of ATP [69], while the stable conformation of the

(hydrolysis-incapable) ADP·VO_4-bound S1 is dominated by the closed, pre-stroke state [70].

The choice of the reaction coordinates is expected to affect the relevance of the resulting statistics to the overall conformational change in reality as well as the efficiency of the sampling. The RMSD as the reaction coordinate, compared to other possibilities more directly connected to structural features, such as the lever arm rotation angle, allows one to steer the global conformational changes without particular biases toward pre-supposed structural features. Its efficiency as explored in Fig. 3 indicates that, for a given strength of constraints, it mainly acts preferentially on larger scale changes such as converter domain rotation than more subtle ones including the approach of the switch-2 to ATP. One might conclude from such trends that the resulting sampling thus contains unphysical biases in light of the expectation that, in reality, it is the set of subtle changes first induced by ATP binding that would subsequently cause the large-scale rotation of converter/lever arm complex. However, it is important to recognize that an umbrella sampling, when performed adequately, only reflects static equilibrium statistics constrained to a particular region of conformational space, and the specific order of the structural changes in which a particular equilibration has been reached is irrelevant. A locus of such constrained quasi-static states then constitutes a possible dynamical trajectory of the protein on a much longer time-scale of the order of milliseconds, which can be modeled by stochastic dynamical formalisms [30].

The steered dynamical trajectory as shown in Fig. 3, in contrast, is not to be interpreted as an accelerated version of the real dynamics, and instead only reflects the convergence properties of the sampling and the nature of the underlying free energy landscapes, which could be manifested by the possible hysteretic behavior. With sufficient amount of sampling, in particular, a set of RMSD reaction coordinates can reveal the existence of the close coupling between the larger-scale and more subtle structural changes: if the chemical "switching" due to the ATP binding induces the lever arm rotation in reality, forcing the rotation to a particular intermediate degree and probing the response of the switching part is an ideal and efficient way to test such mechanisms. The sampled pathway illustrated in Fig. 5 represents the collection of such intermediate states, and considerations of the structural progression as shown in Fig. 6 in principle can test "the pocket closed → lever arm re-primed" hypothesis. In this context, the large degree of fluctuations present in the statistics of the "closed" nucleotide binding pocket shown in Fig. 6 appears to argue against such a tight mechanical coupling.

The use of related or different reaction coordinates in similarly designed sampling will facilitate broader understanding of the coarse-grained dynamics of conformational changes involved. In addition, in completing the sampling of the free energy landscape initiated in this study (Fig. 5), one can consider performing further samplings with constraining potentials different from the particular form adopted here [Eq. (1)]. The resulting histograms then can be recombined collectively using the re-weighting algorithm [39] with their respective potentials. Possibilities of such future studies include the use of varying strengths of the force constants, and the adoption of the *relative* RMSD ($\Delta y = y_1 - y_2$ in this case) instead of the individual RMSDs [33,34].

Acknowledgment

The author thanks Christopher Moss for his help in analyzing the data, Benoît Roux for insightful comments, and Nilesh Banavali for careful reading of the manuscript and suggestions. This work was supported by the University of Nevada, Reno. The computations were performed in part on the National Science Foundation Terascale Computing System at the Pittsburgh Supercomputing Center. Figs. 1 and 2 were generated using PyMol (W.L. DeLaNO, http://www.pymol.org).

References

[1] R.D. Vale, R.A. Milligan, The way things move: looking under the hood of molecular motor proteins, Science 288 (2000) 88–95.
[2] R.W. Lymn, E.W. Taylor, Mechanism of adenosine triphosphate hydrolysis by actomyosin, Biochemistry 10 (1971) 4617–4624.
[3] M.A. Geeves, K.C. Holmes, Structural mechanism of muscle contraction, Ann. Rev. Biochem. 68 (1999) 687–728.
[4] J.A. Spudich, The myosin swinging cross-bridge model, Nat. Rev., Mol. Cell Biol. 2 (2001) 387–392.
[5] R. Cooke, The sliding filament model: 1972–2004, J. Gen. Physiol. 123 (2004) 643–656.
[6] I. Rayment, W.R. Rypniewski, K. Schmidt-Base, R. Smith, D.R. Tomchick, M.M. Benning, D.A. Winkelmann, G. Wesenberg, H.M. Holden, Three-dimensional structure of myosin subfragment-1: a molecular motor, Science 261 (1993) 50–58.
[7] I. Rayment, H.M. Holden, M. Whittaker, C.B. Yohn, M. Lorenz, K.C. Holmes, R.A. Milligan, Structure of the actin–myosin complex and its implications for muscle contraction, Science 261 (1993) 58–65.
[8] R.A. Milligan, Protein–protein interactions in the rigor actomyosin complex, Proc. Natl. Acad. Sci. U. S. A. 93 (1996) 21–26.
[9] K.C. Holmes, I. Angert, F.J. Kull, W. Jahn, R.R. Schröder, Electron cryomicroscopy shows how strong binding of myosin to actin releases nucleotide, Nature 425 (2003) 423–427.
[10] D.M. Himmel, S. Gourinath, L. Reshetnikova, Y. Shen, A.G. Szent-Györgyi, C. Cohen, Crystallographic findings on the internally uncoupled and near-rigor states of myosin: further insights into the mechanics of the motor, Proc. Natl. Acad. Sci. U. S. A. 99 (2002) 12645–12650.
[11] S. Gourinath, D.M. Himmel, J.H. Brown, L. Reshetnikova, A.G. Szent-Györgyi, C. Cohen, Crystal structure of scallop myosin S1 in the pre-power stroke state to 2.6 Å resolution: flexibility and function in the head, Structure 11 (2003) 1621–1627.
[12] C.A. Smith, I. Rayment, X-ray structure of the magnesium(II)·ADP·vanadate complex of the *Dictyostelium discoideum* myosin motor domain to 1.9 Å resolution, Biochemistry 35 (1996) 5404–5417.
[13] R. Dominguez, Y. Freyzon, K.M. Trybus, C. Cohen, Crystal structure of a vertebrate smooth muscle myosin motor domain and its complex with the essential light chain: visualization of the pre-power stroke state, Cell 94 (1998) 559–571.
[14] W. Steffen, J. Sleep, Repriming the actomyosin crossbridge cycle, Proc. Natl. Acad. Sci. U. S. A. 101 (2004) 12904–12909.
[15] E. Eisenberg, L.E. Greene, The relation of muscle biochemistry to muscle physiology, Annu. Rev. Physiol. 42 (1980) 293–309.
[16] S. Fischer, B. Windshügel, D. Horak, K.C. Holmes, J.C. Smith, Structural mechanism of the recovery stroke in the myosin molecular motor, Proc. Natl. Acad. Sci. U. S. A. 102 (2005) 6873–6878.
[17] W. Zheng, B.R. Brooks, Identification of dynamical correlations within the myosin motor domain by the normal mode analysis of an elastic network model, J. Mol. Biol. 346 (2005) 745–759.
[18] W. Zheng, B.R. Brooks, Probing the local dynamics of nucleotide-binding pocket coupled to the global dynamics: myosin versus kinesin, Biophys. J. 89 (2005) 167–178.
[19] M.M. Tirion, Large amplitude elastic motions in proteins from a single-parameter, atomic analysis, Phys. Rev. Lett. 77 (1996) 1905–1908.

[20] W. Zheng, S. Doniach, A comparative study of motor–protein motions by using a simple elastic-network model, Proc. Natl. Acad. Sci. U. S. A. 100 (2003) 13253–13258.
[21] T.J. Minehardt, R. Cooke, E. Pate, P.A. Kollman, Molecular dynamics study of the energetic, mechanistic, and structural implications of a closed phosphate tube in ncd, Biophys. J. 80 (2001) 1151–1168.
[22] J.D. Lawson, E. Pate, I. Rayment, R.G. Yount, Molecular dynamics analysis of structural factors influencing back door Pi release in myosin, Biophys. J. 86 (2004) 3794–3803.
[23] G. Li, Q. Cui, Mechanochemical coupling in myosin: a theoretical analysis with molecular dynamics and combined QM/MM reaction path calculations, J. Phys. Chem., B 108 (2004) 3342–3357.
[24] G. Li, Q. Cui, Analysis of functional motions in Brownian molecular machines with an efficient block normal mode approach: myosin-II and Ca^{2+}-ATPase, Biophys. J. 86 (2004) 743–763.
[25] Y. Liu, M. Scolari, W. Im, H.-J. Woo, Protein–protein interactions in actin–myosin binding and structural effects of R405Q mutation: a molecular dynamics study, Proteins 64 (2006) 156–166.
[26] K.C. Holmes, R.R. Schröder, H.L. Sweeney, A. Houdusse, The structure of the rigor complex and its implications for the power stroke, Philos. Trans. R. Soc. Lond., B Biol. Sci. 359 (2004) 1819–1828.
[27] P. Kollman, Free energy calculations: applications to chemical and biological phenomena, Chem. Rev. 93 (1993) 2395–2417.
[28] T. Simonson, G. Archontis, M. Karplus, Free energy simulations come of age: protein–ligand recognition, Acc. Chem. Res. 35 (2002) 430–437.
[29] S. Bernèche, B. Roux, A microscopic view of ion conduction through the K^+ channel, Proc. Natl. Acad. Sci. 100 (2003) 8644–8648.
[30] H.-J. Woo, C.L. Moss, Analytical theory of the stochastic dynamics of the power stroke in nonprocessive motor proteins, Phys. Rev., E Stat. Phys. Plasmas Fluids Relat. Interdiscip. Topics 72 (2005) 051924.
[31] S. Bernèche, B. Roux, Energetics of ion conduction through the K^+ channel, Nature 414 (2001) 73–77.
[32] S. Sun, A.R. Dinner, D. Chandler, G. Oster, Elastic energy storage in β-sheets with application to F1 ATPase, Eur. Biophys. J. 32 (2003) 676–683.
[33] N.K. Banavali, B. Roux, Free energy landscape of A-DNA to B-DNA conversion in aqueous solution, J. Am. Chem. Soc. 127 (2005) 6866–6876.
[34] N.K. Banavali, B. Roux, The N-terminal end of the catalytic domain of Src kinase Hck is a conformational switch implicated in long-range allosteric regulation, Structure 13 (2005) 1715–1723.
[35] K.P. Ravindranathan, E. Gallicchio, R.M. Levy, Conformational equilibria and free energy profiles for the allosteric transition of the ribose-binding protein, J. Mol. Biol. 353 (2005) 196–210.
[36] H.-J. Woo, B. Roux, Calculation of absolute protein–ligand binding free energy from computer simulations, Proc. Natl. Acad. Sci. U. S. A. 102 (2005) 6825–6830.
[37] G.M. Torrie, J.P. Valleau, Non-physical sampling distributions in Monte-Carlo free-energy estimation – umbrella sampling, J. Comput. Phys. 23 (1977) 187–199.
[38] A.M. Ferrenberg, R.H. Swendsen, Optimized Monte-Carlo data-analysis, Phys. Rev. Lett. 63 (1989) 1195–1198.
[39] S. Kumar, D. Bouzida, R.H. Swendsen, P.A. Kollman, J.M. Rosenberg, The weighted histogram analysis method for free-energy calculations on biomolecules: I. The method, J. Comput. Chem. 13 (1992) 1011–1021.
[40] M. Souaille, B. Roux, Extension to the weighted histogram analysis method: combining umbrella sampling with free energy calculations, Comput. Phys. Commun. 135 (2001) 40–57.
[41] J. Ma, M. Karplus, Molecular switch in signal transduction: reaction paths of the conformational changes in ras p21, Proc. Natl. Acad. Sci. U. S. A. 94 (1997) 11905–11910.
[42] L. Yang, W. Beard, S. Wilson, B. Roux, S. Broyde, T. Schlick, Local deformations revealed by dynamics simulations of DNA polymerase Beta with DNA mismatches at the primer terminus, J. Mol. Biol. 321 (2002) 459–478.
[43] S. Izrailev, S. Stepaniants, M. Balsera, Y. Oono, K. Schulten, Molecular dynamics study of unbinding of the avidin–biotin complex, Biophys. J. 72 (1997) 1568–1581.
[44] B.R. Brooks, R.E. Bruccoleri, B.D. Olafson, D.J. States, S. Swaminathan, M. Karplus, CHARMM: a program for macromolecular energy, minimization, and dynamics calculations, J. Comput. Chem. 4 (1983) 187–217.
[45] A.D. MacKerell Jr., D. Bashford, M. Bellott, R.L. Dunbrack Jr., J.D. Evanseck, M.J. Field, S. Fischer, J. Gao, H. Guo, S. Ha, D. Joseph-McCarthy, L. Kuchnir, K. Kuczera, F.T.K. Lau, C. Mattos, S. Michnick, T. Ngo, D.T. Nguyen, B. Prodhom, W.E. Reiher III, B. Roux, W. Schlenkrich, J.C. Smith, R. Stote, J. Straub, M. Watanabe, J. Wiorkiewicz-Kuczera, D. Yin, M. Karplus, All-atom empirical potential for molecular modeling and dynamics studies of proteins, J. Phys. Chem., B 102 (1998) 3586–3616.
[46] N. Guex, M.C. Peitsch, SWISS-MODEL and the Swiss-PdbViewer: an environment for comparative protein modeling, Electrophoresis 18 (1997) 2714–2723.
[47] W.L. Jorgensen, J. Chandrasekhar, J.D. Madura, R.W. Impey, M.L. Klein, Comparison of simple potential functions for simulating liquid water, J. Chem. Phys. 79 (1983) 926–935.
[48] H.C. Andersen, Molecular-dynamics simulations at constant pressure and/or temperature, J. Chem. Phys. 72 (1980) 2384–2393.
[49] S. Nose, M.L. Klein, Constant pressure molecular dynamics for molecular-systems, Mol. Phys. 50 (1983) 1055–1076.
[50] W.G. Hoover, Canonical dynamics: equilibrium phase-space distributions, Phys. Rev., A 31 (1985) 1695–1697.
[51] T. Darden, D. York, L. Pederson, Particle mesh Ewald: an *N* log *N* method for Ewald sums in large systems, J. Chem. Phys. 98 (1993) 10089–10092.
[52] W.F. van Gunsteren, H.J.C. Berendsen, Algorithms for macromolecular dynamics and constraint dynamics, Mol. Phys. 34 (1977) 1311–1327.
[53] M. Gerstein, A.M. Lesk, C. Chothia, Structural mechanism for domain movements in proteins, Biochemistry 33 (1994) 6739–6749.
[54] A. Houdusse, A.G. Szent-Györgyi, C. Cohen, Three conformational states of scallop myosin S1, Proc. Natl. Acad. Sci. U. S. A. 97 (2000) 11238–11243.
[55] A. Houdusse, V.N. Kalabokis, D. Himmel, A.G. Szent-Gyorgyi, C. Cohen, Atomic structure of scallop myosin subfragment S1 complexed with MgADP: a novel conformation of the myosin head, Cell 97 (1999) 459–470.
[56] M.A. Young, S. Gonfloni, G. Superti-Furga, B. Roux, J. Kuriyan, Dynamic coupling between the SH2 and SH3 domains of c-Src and Hck underlies their inactivation by C-terminal tyrosine phosphorylation, Cell 105 (2001) 115–126.
[57] M. Balsera, S. Stepaniants, S. Izrailev, Y. Oono, K. Schulten, Reconstructing potential energy functions from simulated force-induced unbinding processes, Biophys. J. 73 (1997) 1281–1287.
[58] H. Lu, K. Schulten, Steered molecular dynamics simulations of force-induced protein domain unfolding, Proteins Struct. Funct. Genet. 35 (1999) 453–463.
[59] V. Ortiz, S.O. Nielsen, M.L. Klein, D.E. Discher, Unfolding a linker between helical repeats, J. Mol. Biol. 349 (2005) 638–647.
[60] H. Ohnishi, S. Kojima, K. Katoh, K. Fujiwara, H.M. Martinez, M.F. Morales, Functional transitions in myosin: formation of a critical salt-bridge and transmission of effect to the sensitive tryptophan, Proc. Natl. Acad. Sci. U. S. A. 95 (1998) 6653–6658.
[61] P.B. Conibear, A. Málnási-Csizmadia, C.R. Bagshaw, The effect of F-actin on the relay helix position of myosin II, as revealed by tryptophan fluorescence, and its implications for mechanochemical coupling, Biochemistry 43 (2004) 15404–15417.
[62] M. Kovács, A. Málnási-Csizmadia, R.J. Woolley, C.R. Bagshaw, Analysis of nucleotide binding to *Dictyostelium* myosin II motor domains containing a single tryptophan near the active site, J. Biol. Chem. 277 (2002) 28459–28467.
[63] A. Málnási-Csizmadia, D.S. Pearson, M. Kovács, R.J. Woolley, M.A. Geeves, C.R. Bagshaw, Kinetic resolution of a conformational transition and the ATP hydrolysis step using relaxation methods with a *Dictyostelium* myosin II mutant containing a single tryptophan residue, Biochemistry 40 (2001) 12727–12737.
[64] M. Furch, S. Fujita-Becker, M.A. Geeves, K.C. Holmes, D.J. Manstein, Role of the salt-bridge between switch-1 and switch-2 of *Dictyostelium* myosin, J. Mol. Biol. 290 (1999) 797–809.
[65] A. Málnási-Csizmadia, D.S. Pearson, M. Kovács, R.J. Woolley, M.A. Geeves, C.R. Bagshaw, Kinetic resolution of a conformational transition

and the ATP hydrolysis step using relaxation methods with a *Dictyostelium* myosin II mutant containing a single tryptophan residue, Biochemistry 40 (2001) 12727–12737.
[66] H. Wang, G. Oster, Energy transduction in the F-1 motor of ATP synthase, Nature 396 (1998) 279–282.
[67] J. Xing, J.-C. Liao, G. Oster, Making ATP, Proc. Natl. Acad. Sci. U. S. A. 102 (2005) 16539–16546.
[68] S. Myong, B.C. Stevens, T. Ha, Bridging conformational dynamics and function using single-molecule spectroscopy, Structure 14 (2006) 633–643.
[69] Y. Suzuki, T. Yasunaga, R. Ohkura, T. Wakabayashi, K. Sutoh, Swing of the lever arm of a myosin motor at the isomerization and phosphate-release steps, Nature 396 (1998) 380–383.
[70] W.M. Shih, Z. Gryczynski, J.R. Lakowicz, J.A. Spudich, A FRET-based sensor reveals large ATP hydrolysis-induced conformational changes and three distinct states of the molecular motor myosin, Cell 102 (2000) 683–694.